

# Linear response phonon dynamics of anisotropic black phosphorous monolayer: PAW mediated *ab initio* DFPT calculations

Sushant Kumar Behera and Pritam Deb\*

*Advanced Functional Material Laboratory, Department of Physics,  
Tezpur University (Central University), Tezpur-784028, India.*

(Dated: April 19, 2019)

The first order standard perturbation theory combined with *ab initio* projector augmented wave operator challenges the realization of the standard Sternheimer equation with linear computational efficiency. Using generalized density functional perturbation theory (DFPT) with Boltzmann transport theory (BTE), we describe the electron-phonon interaction in two-dimensional (2D) black phosphorous monolayer. Subsequently, linear response phonon dynamic behaviour in terms of conductivities, seebeck coefficients and transport properties are focused for its thermoelectric application. The analysis reveals the crystal orientation dependence via structural anisotropy and the density of states of the monolayer structure. Momentum dependent phonon population dynamics along with the phonon linewidth are efficient in terms of reciprocal space electronic states. The optimized values of thermal conductivities of electrons and Seebeck coefficients act as driving force to modulate thermoelectric effects. Figure of merit is calculated to be  $\sim 0.074$  at 300 K and  $\sim 0.152$  at 500 K of the MLBP system as a function of the power factor. With the anticipated superior performance, profound thermoelectric applications can be achieved particularly in the monolayer black phosphorous system.

**keywords:** black phosphorous monolayer, linear response dynamic behavior, phonon population

## I. INTRODUCTION

Quantum confinement effect plays primary role in low dimensional semiconductors to perform efficiently as thermoelectric materials [1]. The carrier energy tunes rapidly the electronic states of such reduced dimensional systems. As a result, Seebeck coefficient is automatically enhanced for better performance [2]. Figure of merit (ZT), a dimensionless factor, quantifies thermoelectric device efficiency relating the Seebeck coefficient (i.e. the thermopower) to electronic thermal conductivity. The lesser thermal conductivity value along with relatively higher thermopower and electrical conductivity values are robust aspects for high efficiency thermoelectric materials. The efficiency improvement is mainly controlled due to the sharp peaked electronic density of states (DOS). Nanotechnology has been applied extensively to improve the thermoelectric performance since the past two decades [3, 4]. Few of the nanostructures [5–8], 2-dimensional electron gas (2 DEG) [9, 10] and nanowires [11] have all been reported for superior thermoelectric and transport properties. However, it is difficult task to control the dimensional scaling of such structures to achieve superior performance cost effectively. In the line of search for effective structures as enriched thermoelectric and phonon transport performance, natural two dimensional (2D) materials with finite bandgap (i.e. semiconductors or semimetals), low energy dispersion, high carrier mobility and minimized phonon modes are considered as suitable candidates [12–18].

Recently, monolayer black phosphorous (MLBP) known as an allotrope of bulk black phosphorous, a 2D material family, has appeared in this line of research [19–23]. MLBP possesses puckered honeycomb lattice of phosphorous atoms with low symmetry and highly anisotropy resulting many interesting and applied active benefits of the structure [24–27]. The Seebeck coefficient and phonon modes are directly dependent on this anisotropic electronic structure resulting better thermoelectric and phonon transport performance. In this aspect, experimental findings on multi-layer or monolayer black phosphorous have been reported to realize the theoretical predictions [28–31]. More recently, electron-phonon interaction in phosphorene has been performed via first-principle calculations based on DFPT and Wannier interpolation with norm conserving pseudo potential [32].

In the line of understanding, first order Kohn-Sham equations written in the form of a perturbation series are used to realize the basic physics behind standard perturbation theory of Sternheimer equation [33] in the perspective of *ab initio* DFPT method through self-consistency field. Besides, first order Kohn-Sham Hamiltonian is linearly dependent on electron wave function in strongly correlated electron systems like 2D material sheet resulting manifold coupling between conduction and valence bands [34]. Interestingly, projector augmented wave operator is the only option to express such linear dependency in case of the perturbation stage to validate the Sternheimer equations. Interestingly, this first order response of the Kohn Sham Hamiltonian will support to implement the projector augmented wave pseudopotential based DFPT algorithm to calculate thermal and phonon responses with linear computational

---

\* Corresponding Author: pdeb@tezu.ernet.in

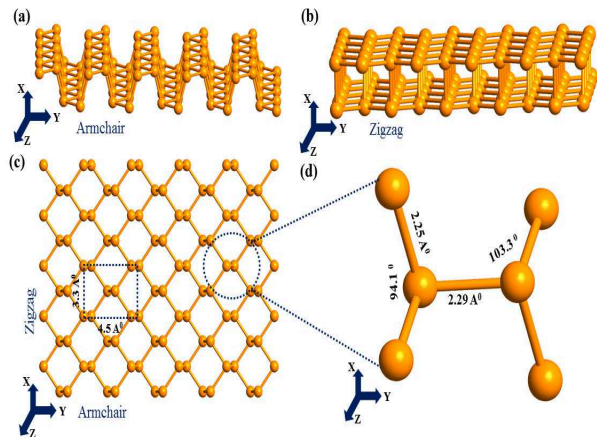


FIG. 1. The optimized geometry of phosphorene monolayer in (a) armchair and (b) zigzag direction shown as side view. The surface aerial view of the monolayer sheet from both the direction shown in (c) and the angle and bond length among the phosphorous atom in (d).

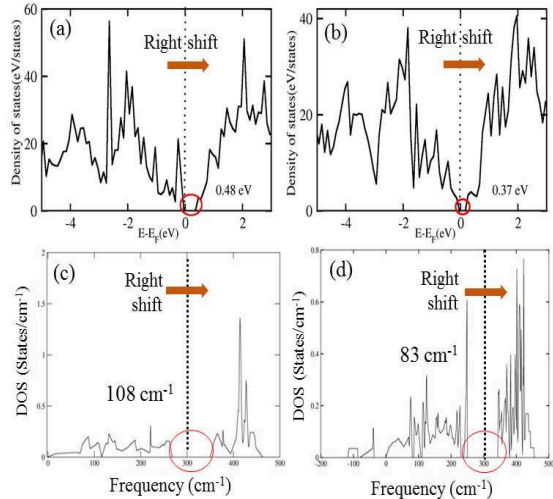


FIG. 2. The distribution of electronic density of states (DOS) of the monolayer at (a) 300 K and (b) 500 K. The dotted black line represents the Fermi level and the red dotted circle shows the closing of gap due to Increase in temperature. The distribution due to phonon states shown at (c) 300 K and (d) 500 K of the same optimized structure. The dotted black line presents the frequency line where states are zero.

efficacy in MLBP system. Theoretically, we are still lacking to implement the linear response phonon dynamics of in 2D monolayer sheets of anisotropic materials in the framework of PAW based DFPT technique. Thus, stimulating research endeavor can be implemented to evaluate the phonon mediated dynamic behaviour and potential thermoelectric performance of MLBP.

In this manuscript, we use *ab initio* DFT with projector augmented wave (PAW) pseudopotential

method supported by Perdew-Burke-Ernzerhof generalized gradient approximation (PBE-GGA) functional to predict electronic and linear response phonon transport behaviour, which self-consistently takes into account for such anisotropic materials. In the context of anisotropic semiconductors, it is interesting to know the feasibility of PAW pseudopotential based DFPT method to analyse the linear phonon dynamics, which presents the characteristic coupling between conduction and valence bands. We address specifically such problem in this current simulation work. Here, BTE is implemented for thermoelectric properties taking the Boltztrap code. The Seebeck coefficient, electronic thermal conductivities, carrier mobility and power factor are considered during the calculation. Moreover, the linear response phonon interaction and dynamic behaviour are calculated for MLBP including the phonon population density with respect to the reciprocal k space symmetry points. Our results, obtained from projector operators and generalized gradient functional in the monolayer sheet, are consistent and superior than the previously reported electron-phonon interaction [32] and thermal transport [31] data showing that the momentum-resolved phonon mediated linear response behaviour of MLBP through self-consistent *ab initio* DFPT calculations.

## II. METHODOLOGY

The electronic structure of ML black phosphorous is studied using DFT calculation using Quantum Espresso codes [35] along with PAW pseudopotential [36] and the PBE functional within the generalized gradient approximation (GGA) [37]. The van der Waals (vdW) interaction has been considered for the monolayer structure [38, 39]. A Monkhorst mesh of  $9 \times 9 \times 1$  k-points is used for geometry optimization with 540 eV as plane wave cutoff energy. Optimization iteration process is followed until the total force converged to  $\leq 0.001 \text{ eV}\text{\AA}^{-1}$ . Supercells with lattices of  $12 \text{ \AA}$  in the z-direction is considered to neglect the periodic interaction among the surface images of the monolayer sheet structures. We use  $27 \times 27 \times 1$  k-mesh for electronic structure calculations. The phonon mode related simulations are performed within the framework of density functional perturbation theory [40] with  $27 \times 27 \times 1$  k point mesh. The transport phenomena has been studied using Boltzmann transport equation (BTE) [41].

## III. RESULTS AND DISCUSSION

The optimized monolayer geometries are determined using quasi Newtonian algorithm. The structures of the layers are shown in Fig. 1. To understand the origin and control of electron states and phononic states at active sites in monolayer and their distribution, the

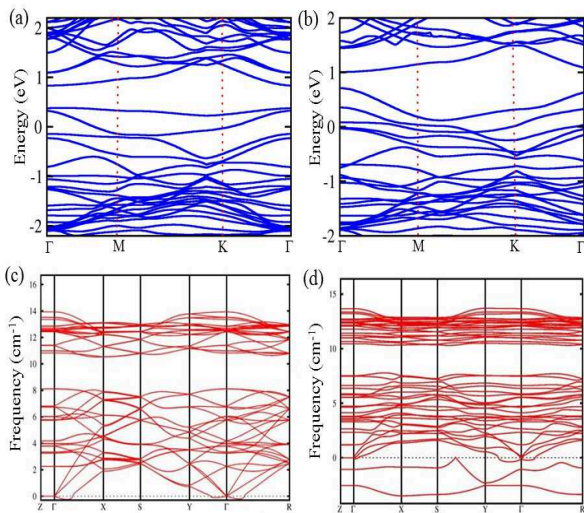


FIG. 3. Electronic band structure of (a) 300 K and (b) 500 K of the monolayer phosphorene. The high symmetry points are  $\Gamma$ , M, K and  $\Gamma$  in reciprocal space. Phononic band structure of the same monolayer at (c) 300 K and (d) 500 K. The high symmetric frequency points are taken Z,  $\Gamma$ , X, S, Y,  $\Gamma$  and R in reciprocal space.

total densities of states (TDOSs) and phonon density of states are performed. Overlapping states are observed from the plots of density of states (Fig. 2) showing the active behavior near the Fermi region and the gap near to the active sites. Presence of localized electrons on the P edge of monolayer sheet has contributed to the overlapping states at Fermi level within conduction band with confinement and delocalization of the phosphorous (P) atoms, resulting the dynamic behaviour of the sites.

The electronic (DOS) (shown in Fig. 2 (a) and (b)) with step-like features are observed near the Fermi level and a slight right shifting upon increasing temperature to 500 K because of highly anisotropic behaviour. We observe similar horizontal level in optimum band edges of both conduction and valence band laterally zigzag direction indicating possibility to improve the value of Seebeck coefficient. This potential finding is worthy enough for the 2D monolayer as thermoelectric material, unlike its bulk counterpart (i.e. black phosphorus).

Optical phonon contribution is significantly low in the phonon density of states (Fig. 2 (c) and (d)). We notice slight peak shifting near the band edges from 108 to 83  $\text{cm}^{-1}$ , which is occurred due to anisotropic band structure of MLBP. To correlate the bands due to electronic states distribution and phonon states with DOS pattern, we have plotted the band diagram in both cases of electronic band and phononic bands (shown in Fig. 3). The band gap is corroborated with its states calculated from DOS pattern.

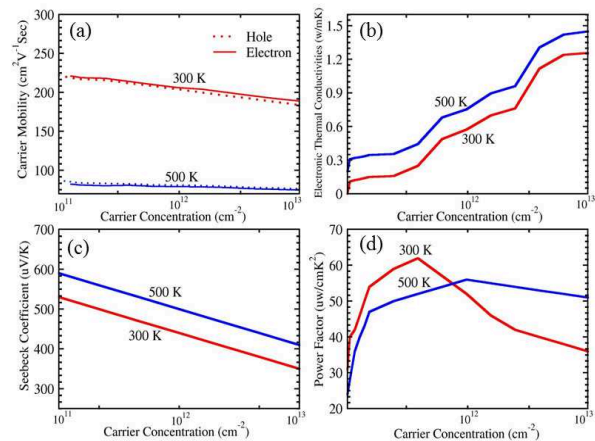


FIG. 4. The calculated (a) carrier mobility, (b) electronic thermal conductivity, (c) Seebeck coefficient and (d) thermo-electric power factor along the zigzag direction of MLBP at two temperatures.

The electrons and hole mobilities are plotted as a function of carrier concentration from the shifting of the Fermi level at room temperature (Fig. 4(a)). The phonon mediated carrier mobility of MLBP is  $\sim 212 \text{ cm}^2/\text{Vs}$  at 300 K corroborating with experimentally verified results of few layers of BP [42]. In Fig. 4(b) we present the calculated electronic thermal conductivity of the MLBP with a higher chance of predictability at higher temperature.

In Fig. 4 ((c) and (d)), the Seebeck coefficient and power factor have been plotted as a function of carrier concentrations at 300 and 500 K. The Seebeck coefficient is dominant and the thermoelectric power factor achieves 60  $\text{W}/\text{cm}\cdot\text{K}^2$  at room temperature. The power factor values at 300 K and 500 K have been taken to calculate the figure of merit of the material as thermoelectric application. The thermoelectric materials are defined by the figure of merit ( $ZT$ ), given as  $ZT = S^2 \sigma k^{-1} \Delta T$ , depending on seebeck coefficient ( $S$ ), electrical conductivity ( $\sigma$ ), electronic thermal conductivity ( $k$ ) and the temperature gradient ( $\Delta T$ ). The formula for  $ZT = (\text{PF}) \cdot k^{-1} \Delta T$  is more simplified by considering ( $S^2 \sigma$ ) as power factor (PF) at the particular temperature gradient to generate electricity [43, 44]. The optimal values of  $ZT$  is calculated to be approximately  $\sim 0.074$  at 300 K and  $\sim 0.152$  at 500 K for the MLBP.

Contributions from the phonon modes in case this 2D system is ignored due to the inversion symmetry. Fig. 5 (a) shows phonon band structure along the high-symmetry and population density of each phonon mode (Fig. 5(b)). The phonon density is varying significantly at different symmetric points for all phonon branches of the ML structure at 300 and 500 K along the zigzag direction.

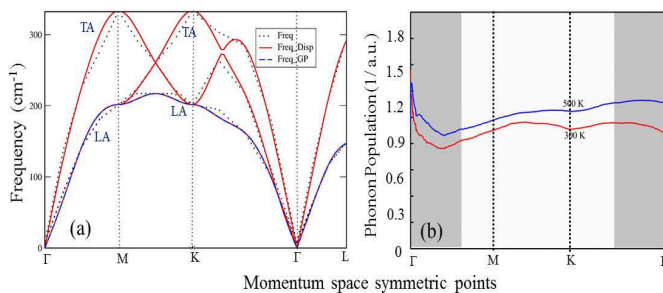


FIG. 5. (a) Phonon band structure along the momentum space high-symmetry ( $\Gamma$ -M-K- $\Gamma$ ) points. The solid lines are summed over all phonon branches and the dashed line is the sum of all acoustic (i.e. longitudinal acoustic (LA) and transverse acoustic (TA)) branches. (b) momentum-resolved first-principles based calculations of phonon population at two different electronic temperatures, the gray areas indicate the q range.

We calculate the variation in individual phonon population density as a function of their reciprocal k space and reveal the transport property along the zigzag direction (Fig. 5(b)). The optimized phonon density is determined to be 0.95 at room temperature and 1.12 at 500 K near M and K points. Here, the results estimate the relative effectiveness of low dimensional structures in affecting their transport properties. The comparison of the linear response phonon population and the phonon band structures (Fig. 5) shows analogous momentum space dependency. Quantitatively, the calculated phonon population is enriched by a factor of 7 on increasing the electronic temperature to 500 K. Here, electrons relax to the CBM by consequent phonon scattering. The electronic temperature changes dynamically adjusting the phonon coupling strength with a finite CBM frequency difference at M and K points of more than  $300 \text{ cm}^{-1}$  (Fig. 5(a)). Therefore,

the quantitative difference of the phonon population dynamics and the reciprocal space band structure are in good agreement with each other.

#### IV. CONCLUSION

In summary, the momentum-resolved phonon mediated linear response behaviour can be understood by examining the phonon scattering of MLBP from first principle calculations taking PAW pseudopotential and PBE-GGA functional. Carrier mobility and optical phonon contribution are supporting the band shifting and thermoelectric functionality along zigzag direction due to highly anisotropic nature of the monolayer surface. The phonon scattering rates reveals the linear scale directional dependence of the lattice dynamics. The estimated carrier mobility and power factor are found to be  $212 \text{ cm}^2/\text{Vs}$  and around  $60 \text{ W/cm-K}^2$  at room temperature, respectively, which are significant for intrinsic transport property. Increasing trend of figure of merit and the reduced value of seebeck coefficient supports monolayers to be more favorable than their bulk counterpart, indicating the positiveness of nanostructuring MLBP for thermoelectric performance. The results in this study justifies superior performance in thermoelectric applications of monolayer black phosphorous.

#### ACKNOWLEDGMENTS

SKB acknowledges DST, Govt. of India for providing INSPIRE Fellowship. The authors acknowledge Tezpur University for providing HPCC facility.

- 
- [1] V. P. Gusynin and S. G. Sharapov, Phys. Rev. Lett. **95**, 146801 (2005).
  - [2] S. Das and J. Appenzeller, Appl. Phys. Lett. **103**, 103501 (2013).
  - [3] Y. Yoon and S. Salahuddin, Appl. Phys. Lett. **101**, 263501 (2012).
  - [4] J. T. P. et al, J. Phys.: Condens. Matter **29**, 473001 (2017).
  - [5] J. C. Jamieson, Science **139**, 1291 (1963).
  - [6] M. Elahi and M. Pourfath, J. Phys.: Condens. Matter **30**, 225701 (2018).
  - [7] X. S. L. D. Hicks, T. C. Harman and M. S. Dresselhaus, Phys. Rev. B **53**, R10493 (1996).
  - [8] T. C. R. Venkatasubramanian, E. Siivola and B. Quinn, Nature **413**, 597602 (2001).
  - [9] J. C. P. Zhao and J. Guo 2009 Nano Lett. 9, Nano Lett. **9**, 684 (2009).
  - [10] R. R. et al, J. Phys.: Condens. Matter **27**, 313201 (2015).
  - [11] K. M. P. J. P. Small and P. Kim, Phys. Rev. Lett. **91**, 256801 (2003).
  - [12] C. L. Kane and E. J. Mele 2005 Phys. Rev. Lett. **95**, Phys. Rev. Lett. **95**, 226801 (2005).
  - [13] P. A. L. D. A. Abanin and L. S. Levitov, Phys. Rev. Lett. **98**, 156801 (2007).
  - [14] P. D. S. K. Behera and A. Ghosh, RSC Adv. **7**, 31393 (2017).
  - [15] P. D. S. K. Behera and A. Ghosh, Chemistry Select **2**, 3657 (2017).
  - [16] P. D. S. K. Behera and A. Ghosh, Phys. Chem. Chem. Phys. **18**, 23220 (2016).
  - [17] J. Debdeep and K. Aniruddha 2007 98, Phys. Rev. Lett. **98**, 136805 (2007).
  - [18] S. S. Y. Du, C. Ouyang and M. Lei, J. Appl. Phys. **107**, 093718 (2010).
  - [19] K. S. N. et al, Proc. Natl Acad. Sci. USA **102**, 10451 (2005).

- [20] X. K. C. et al, J. Phys.: Condens. Matter. **30**, 155702 (2018).
- [21] R. Bistritzer and A. H. MacDonald, Phys. Rev. Lett. **102**, 206410 (2009).
- [22] L. J. L. T. J. M. D. Jariwala, V. K. Sangwan and M. C. Hersam, ACS Nano **8**, 1102 (2014).
- [23] X. X. et al, J. Phys.: Condens. Matter **28**, 483001 (2016).
- [24] Y. L. V. Tran, R. Soklaski and L. Yang 2014 Phys. Rev. B **89**, Phys. Rev. B **89**, 235319 (2014).
- [25] P. W. W. D. J. M. J. Liu, T. H. Hsieh, Nat. Mater. **13**, 178 (2014).
- [26] W. F. C. C. Liu and Y. Yao, Phys. Rev. Lett. **107**, 076802 (2011).
- [27] F. H. L. K. et al, Nat. Nanotechnol. **9**, 780 (2014).
- [28] L. L. L. C. Z. H. M. D. F. W. Han, W. Xu and F. M. Peeters, Phys. Rev. B **95**, 115436 (2017).
- [29] A. C. A. S. Rodin and A. H. C. Neto, Phys. Rev. Lett. **112**, 176801 (2014).
- [30] Z. Q. S. Y. Y. M. H. G. Qin, Q. B. Yan and G. Su, Phys. Chem. Chem. Phys. **17**, 4854 (2015).
- [31] T. A. d. S. P. L. Craco and S. Leoni, Phys. Rev. B **96**, 075118 (2017).
- [32] B. Q. M. S. D. B. Liao, J. Zhou and G. Chen, Phys. Rev. B **91**, 235419 (2015).
- [33] R. M. Sternheimer, Phys. Rev. **96**, 951 (1954).
- [34] S. Y. Savrasov and O. K. Andersen 1996, Phys. Rev. Lett. **77**, Phys. Rev. Lett. **77**, 4430 (1996).
- [35] P. G. et al, J. Phys.: Condens. Matter **21**, 395502 (2009).
- [36] P. E. Blchl, Phys. Rev. B **50**, 17953 (1994).
- [37] K. B. J. P. Perdew and M. Ernzerhof, Phys. Rev. Lett. **77**, 3865 (1996).
- [38] A. A. R. C. N. Ferri, R. A. DiStasio Jr. and A. Tkatchenko, Phys. Rev. Lett. **114**, 176802 (2015).
- [39] P. G. et al, J. Phys.: Condens. Matter **29**, 465901 (2017).
- [40] A. D. C. S. Baroni, S. de Gironcoli and P. Giannozzi, Rev. Mod. Phys. **73**, 515 (2001).
- [41] A. J. H. McGaughey and M. Kaviani, Phys. Rev. B **69**, 094303 (2004).
- [42] G. L. et al, Phys. Rev. B **96**, 155448 (2017).
- [43] G. C. C. W. C. H. S. Kim, W. Liu and Z. Ren, Proc. Natl. Acad. Sci. USA **112**, 8205 (2015).
- [44] G. J. Snyder and A. H. Snyder, Energy Environ. Sci. **10**, 2280 (2017).